Obrabotka metallov –
Metal Working and Material Science

Journal homepage: http://journals.nstu.ru/obrabotka_metallov

Fabrication, characterization and performance evaluation of zinc oxide doped nanographite material as a humidity sensor

*Farrukh Waheed [1, a], Amtul Qayoom [2, b], Muhammad Faizan Shirazi [3, c, *]*

[1] Department of Computer Science, Usman Institute of Technology University, ST-13, Abul Hasan Isphahani Road, Block 7, Gulshan-e-Iqbal, Karachi, 75300, Pakistan

[2] Department of Chemistry, NED University of Engineering and Technology, University Road, Karachi, 75270, Pakistan

[3] Department of Electronic Engineering, NED University of Engineering and Technology, University Road, Karachi, 75270, Pakistan

[a] https://orcid.org/0009-0004-6527-0965, ✉ fwbaig@uitu.edu.pk; [b] https://orcid.org/0000-0003-0149-2177, ✉ amtulq@neduet.edu.pk;
[c] https://orcid.org/0000-0002-4488-8860, ✉ faizanshirazi@neduet.edu.pk

ARTICLE INFO

ABSTRACT

Introduction. The growing demand for real-time environmental monitoring technologies has led to increased interest in high-performance humidity sensors with rapid response, high sensitivity, and long-term stability. Zinc oxide (*ZnO*) is a widely used semiconducting oxide material for such applications due to its chemical stability and sensitivity to humidity variations. However, its performance can be further enhanced through material engineering. This study investigates the doping of *ZnO* nanoparticles with nanographite material (*NGM*) to improve humidity-sensing characteristics. The **purpose of the work** is to develop ZnO–NGM nanocomposite-based capacitive humidity sensors with improved response/recovery time and sensitivity by modifying the electronic and surface properties of *ZnO* through *NGM* doping. **Research methods.** ZnO–NGM nanocomposites with varying *NGM* content (1 wt.%, 2 wt.%, 4 wt.%, 5 wt.%, and 10 wt.%) were synthesized via a chemical precipitation route. The optical behavior of pure *ZnO* was analyzed using *UV–Vis* spectroscopy, which revealed a sharp absorption edge at 367 nm, indicating a bandgap near 3.3 eV. Structural and morphological properties were examined using X-ray diffraction (*XRD*) and scanning electron microscopy (*SEM*), confirming *NGM* integration and enhanced surface porosity. The composite sensing films were deposited onto *FTO*-coated glass substrates using the 'doctor blade' method to fabricate the capacitive sensors. The sensing performance was evaluated in a nitrogen-controlled chamber over a relative humidity (*RH*) range of 10% to 95%, with capacitance measurements recorded across a frequency range of 10 kHz to 1 MHz. **Results and discussion.** Among all tested compositions, the 4 wt.% *NGM*-doped *ZnO* sensor demonstrated the best performance, with a rapid response time of 4.0 s, a recovery time of 6.2 s, and excellent sensitivity. These improvements are attributed to enhanced surface conductivity and more active adsorption-desorption kinetics due to *NGM*. The developed sensors show strong potential for integration in real-time environmental monitoring systems, industrial automation, and smart home humidity control applications. The incorporation of nanographite into *ZnO* matrices significantly enhances humidity-sensing capabilities. The ZnO–NGM composite, particularly at 4 wt.% doping, offers a promising pathway for the development of next-generation, high-efficiency humidity sensors.

Introduction

Humidity sensors have significant applications in agriculture, food technology, medical diagnostics, and environmental monitoring due to the increasing need for real-time, accurate measurements in state-of-the-art intelligent systems. Low power consumption, rapid response, stability, and low cost are key requirements of contemporary sensors [1-2]. A research paper discusses a flexible humidity sensor that can sense minor changes in breath for medical use [3-4]. Similarly, another study presents highly sensitive humidity sensors constructed with carbon nanotube composites, emphasizing rapid response times suitable

* Corresponding author
Shirazi Muhammad Faizan, Ph.D. (Engineering)
Department of Electronic Engineering,
NED University of Engineering and Technology,
75270, University Road, Karachi, Pakistan
Tel.: +92-21-99261261-8 ext. 2215, **e-mail:** faizanshirazi@neduet.edu.pk

for various environments [5]. Another study showcases the efficacy of using encapsulated ionic liquids in nanostructured frameworks for enhanced humidity sensing capabilities, reinforcing the trend of leveraging novel materials for improved performance [6]. Self-powered and biocompatible sensors are increasingly under research, and graphene oxide-based humidity sensors promise energy-efficient, sensitive detection [7]. An *rGO:MoS₂*-based temperature-integrated humidity sensor proves the versatility of its applications in reality [8]. Research investigating TiO_2-SnS_2 heterostructures for use in humidity sensors emphasizes the advantages of nanoarchitectures in enhancing sensor performance [9-12].

Metal oxide humidity sensors, like *ZnO*, *TiO₂*, and *SnO₂*, are commonly researched for their stability and moisture sensitivity and measure humidity through capacitance or resistance changes after water adsorption [1-3]. These characteristics make *ZnO* an exceptionally versatile material for fabricating high-performance humidity sensors. Furthermore, the tunable electronic properties of *ZnO*, achieved through doping with various elements and precise nanostructuring, allow for fine-tuning of the sensor's performance to meet specific application requirements [13-14]. Nanographite material (*NGM*), which is green synthesized from orange and lemon peels, improves *ZnO*-based humidity sensors with enhanced charge transfer, adsorption ability, and stability, thereby supporting sustainable nanotechnology [10].

Recent studies emphasize the need for improvements in response times and recovery cycles in humidity sensors, highlighting that these parameters are critical for effective real-time applications [15-16]. A study conducted by *Ullah et al.* demonstrated that by integrating nanographite with metal oxides, the resulting sensor achieved significant reductions in response and recovery times, addressing previous limitations [17]. Furthermore, research by *Chaudhary et al.* emphasized the importance of utilizing innovative architectures and materials to enhance the sensor's overall performance metrics [18]. Moreover, the study by *Li et al.* outlined the effectiveness of doping *ZnO* with nanographite in improving the sensor's performance at various humidity levels, showcasing its potential for practical application [13]. The tunability of electronic properties through the introduction of nanographite provides researchers with new avenues for enhancing sensor reliability and efficiency, making them more suitable for integration into *IoT* and smart technology frameworks [14]. Despite the aforementioned studies, there is still a need for enhancement of zinc oxide-based nanosensors for lower response times.

Despite these advancements, there is still a clear need to develop *ZnO*-based humidity sensors with lower response times, improved stability, and environmentally friendly, scalable fabrication techniques. Specifically, the integration of *NGM* into *ZnO* using cost-effective and simple chemical methods remains relatively underexplored.

The present work aims to address these limitations by synthesizing *ZnO–NGM* nanocomposites via a low-cost chemical precipitation method. The nanocomposites are deposited onto fluorine-doped tin oxide (*FTO*) substrates using the doctor-blade technique to fabricate capacitive-type humidity sensors. The use of *NGM* is expected to improve the sensor's performance by enhancing electrical conductivity and water molecule interaction at the surface. Comprehensive characterization, including *UV–Vis* spectroscopy, *SEM*, *XRD*, and *FTIR*, was conducted to analyze the structural, optical, and chemical features of the material. Humidity sensing was evaluated through capacitance and impedance analysis in a nitrogen-controlled environment across *RH* levels from 10% to 95% [19]. Capacitance and impedance measurements assessed the humidity sensing capability of these synthesized sensors. The results contribute to the development of improved humidity nanosensors, with implications for environmental monitoring, healthcare, and industrial automation.

Investigation techniques

Materials and Methods

High-purity analytical-grade zinc acetate (*Zn(CH₃COO)₂*), ammonium hydrogen carbonate (*NH₄HCO₃*), nanographite material (*NGM*), ethanol (analytical grade), and ethyl cellulose were sourced from *BDH*, *Merck*, and *Sigma-Aldrich*. Deionized water was employed throughout the synthesis and washing to avoid ionic or particulate contamination. Fluorine-doped tin oxide (*FTO*) glass substrates were employed for

device fabrication. Copper and silver electrodes were used for device fabrication. Before application, all the substrates and components were properly cleaned with a *Liquinox* detergent solution (*Alconox Inc.*) and then rinsed with analytical-grade acetone (*Sigma-Aldrich*) to remove organic impurities and provide a clean surface free of contaminants.

### *Synthesis of zinc oxide (ZnO) nanoparticles via chemical precipitation*

10 ml of 1.5 mol/L zinc nitrate ($Zn(NO_3)_2$) was slowly added to 10 ml of 2.25 mol/L ammonium carbonate (($NH_4)_2CO_3$) solutions with magnetic stirring. A white $ZnCO_3$ precipitate confirmed successful synthesis [1].

The chemical reactions involved are:

$$Zn(NO_3)_2S + (NH_4)_2CO_3 \rightarrow ZnCO_3 \downarrow + 2\,NH_4NO_3$$
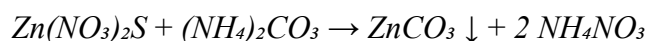
The precipitate was collected through vacuum filtration with an appropriate pore filter paper to remove liquid by-products and unreacted precursors. It was washed three times with deionized water. The high volatility of ethanol allowed for quicker drying, yielding a pure precipitate to be used in subsequent *ZnO* nanoparticles synthesis.

The $ZnCO_3$ was filtered and dried at 80°C to evaporate residual solvents without agglomeration, maintaining the nanostructure. The dried precursor powder was calcined at 550°C for 2 hours using a muffle furnace, promoting the thermal decomposition of $ZnCO_3$ to *ZnO*.

$$ZnCO_3 \rightarrow ZnO + CO_2$$
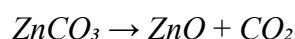
Doping of ZnO nanoparticles with nanographite (NGM)

Both *ZnO* and *NGM* were initially in powdered form. Both were dispersed separately in ethanol. The *NGM* suspension was then added dropwise to the *ZnO* solution with continuous stirring for 25 minutes to achieve good mixing. *ZnO* to *NGM* weight ratios were varied to obtain 99:1, 98:2, 97:3, 96:4, 95:5, and 90:10 composites. Next, 10 mL of ethanol was further added as a dispersant to facilitate dispersion and to lower surface tension. For the powder form, the paste was dried at 50–70 °C for 1–2 hours to prevent nanoparticle agglomeration and ensure equal *NGM* distribution.

Fabrication of the humidity sensor

FTO glass substrates were sequentially sonicated in detergent, deionized water, acetone, and ethanol to clean them for the best adhesion and consistent sensor performance. *ZnO* nanoparticles doped with *NGM* were combined with ethanol to produce a viscous paste appropriate for doctor-blading. The paste was cast on cleaned FTO substrates by the doctor-blade method and thermally treated at 150 °C for 1 hour for the improvement of film adhesion, evaporation of the residual solvents, and durability. Fig. 1 shows the *ZnO* doped with *NGM* paste on a *FTO* glass substrate. Figs. 1, *a* and 1, *b* show the *ZnO* doped with *NGM* paste on a *FTO* glass substrate.

For further stabilization of the film and to increase its stability, ethyl cellulose (2–10 wt %) was dissolved in ethanol with constant stirring to produce a uniform solution. This was added progressively into the *ZnO* doped *NGM* paste to achieve optimal coating. Incorporation of ethyl cellulose enhanced adhesion, surface smoothness, and mechanical strength to yield stable, uniform nanocomposite layers for humidity sensing [1, 30].

Results and Discussion

Structural and morphological analysis

The optical properties of the as-synthesized *ZnO* nanoparticles were investigated by *UV–Vis* spectroscopy. The absorption spectrum, shown in Fig. 2, shows a sharp and intense absorption edge at around 367 nm, which is consistent with the intrinsic bandgap transition of *ZnO*. The *UV–Vis* was performed using a *UV-*
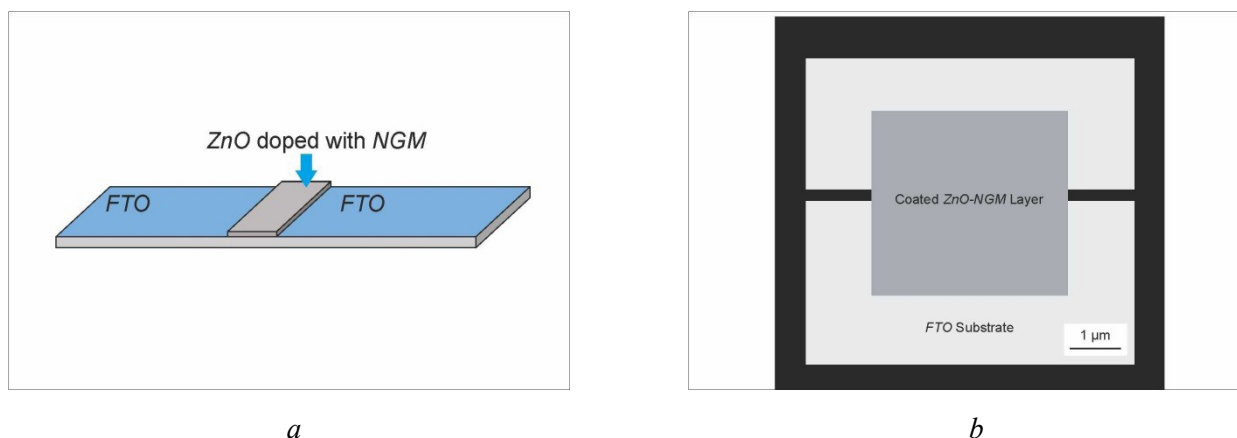
a

b

Fig. 1. (a) Side-view of *ZnO–NGM* paste on *FTO* substrate, (*b*) Top view showing surface morphology
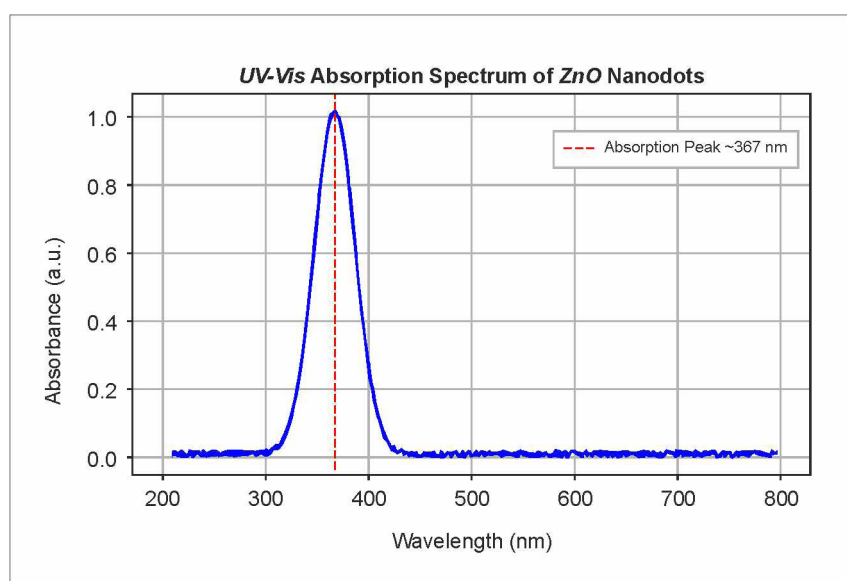

Fig. 2. UV–Vis absorption spectrum of as-synthesized *ZnO* nanoparticles exhibiting a narrow absorption peak at 367 nm, suggesting a direct bandgap transition and validating nanoscale crystallinity for optoelectronic and sensing purposes

1800 SHIMADZU. This peak is related to a direct bandgap energy of about 3.38 eV, which verifies the semiconducting nature of the *ZnO* nanostructures. The blue shift of the absorption edge from the bulk *ZnO* (~375 nm) as shown in Fig. 2 indicates a quantum confinement effect, a signature of the nanoscale size of the particles. The sharp and steep slope of the absorption also indicates the high crystallinity and purity of the as-synthesized *ZnO* nanoparticles. These optical characteristics render the material particularly apt for humidity sensing, *UV* photodetectors, and other optoelectronic uses, where there is a need for a fast and sensitive response to environmental stimuli.

SEM images (in Fig. 3) indicated well-distributed *ZnO* nanoparticles with well-defined morphology. Higher magnification images indicated well-dispersed particles with increased surface texture and observable agglomeration in certain areas. The scanning was performed using a *JEOL JSM-6490A* scanning electron microscope (*JEOL Ltd.*, Japan). The addition of *NGM* enhanced the surface roughness and uniformity of distribution. The increased roughness increases the number of active sites, which aids in better water molecule adsorption, which is essential for enhanced humidity sensing performance [3].

XRD patterns showed a well-crystallized hexagonal structure of *ZnO* (quartzite). Peak broadening and minor shifts were noted with increasing *NGM* concentration, which are signs of successful *NGM*
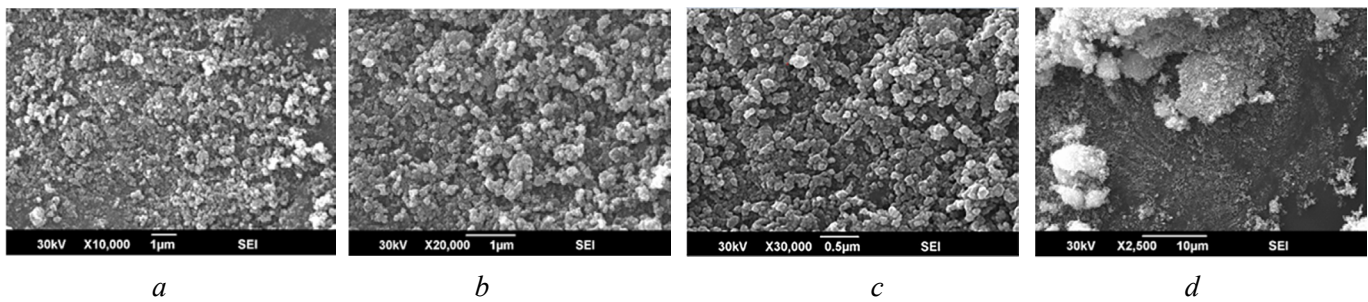
Fig. 3. Scanning electron microscopy (*SEM*) images of *ZnO* nanoparticles at different magnifications:
a – 10,000×; *b* – 20,000×; *c* – 30,000×; *d* – 2,500×

incorporation. These shifts are most likely due to lattice strain, resulting in smaller crystallite size and the creation of structural defects that increase surface area and water adsorption capacity [3].

Fig. 4 shows *XRD* patterns of different samples. Sample 1 (*B-3K953*) showed several peaks between 20° and 80° (2θ), with major peaks near 30°, 40°, and 50°, relating to *ZnO* and traces of impurities. Sample 2 (*B-3K954*) had sharper peaks, indicating better crystallinity. Sample 3 (*B-3K955*) had intermediate crystallinity. All the samples consisted of mostly the *ZnO* phase, while peak width and intensity variations were due to variations in crystallinity due to doping and processing conditions [3].

FTIR spectra verified the inclusion of *NGM* within the *ZnO* matrix Fig. 5. A typical *Zn–O* stretching vibration around 450 cm^{-1} ensured the presence of *ZnO*. Peaks around 1,570 cm^{-1} (*C=C*) and 1,730 cm^{-1} (*C=O*) ensured the occurrence of carbon-containing functional groups in *NGM*. A broad band around ~3,400 cm^{-1} indicated *O–H* stretching, due to hydroxyl groups, responsible for adsorption of water.

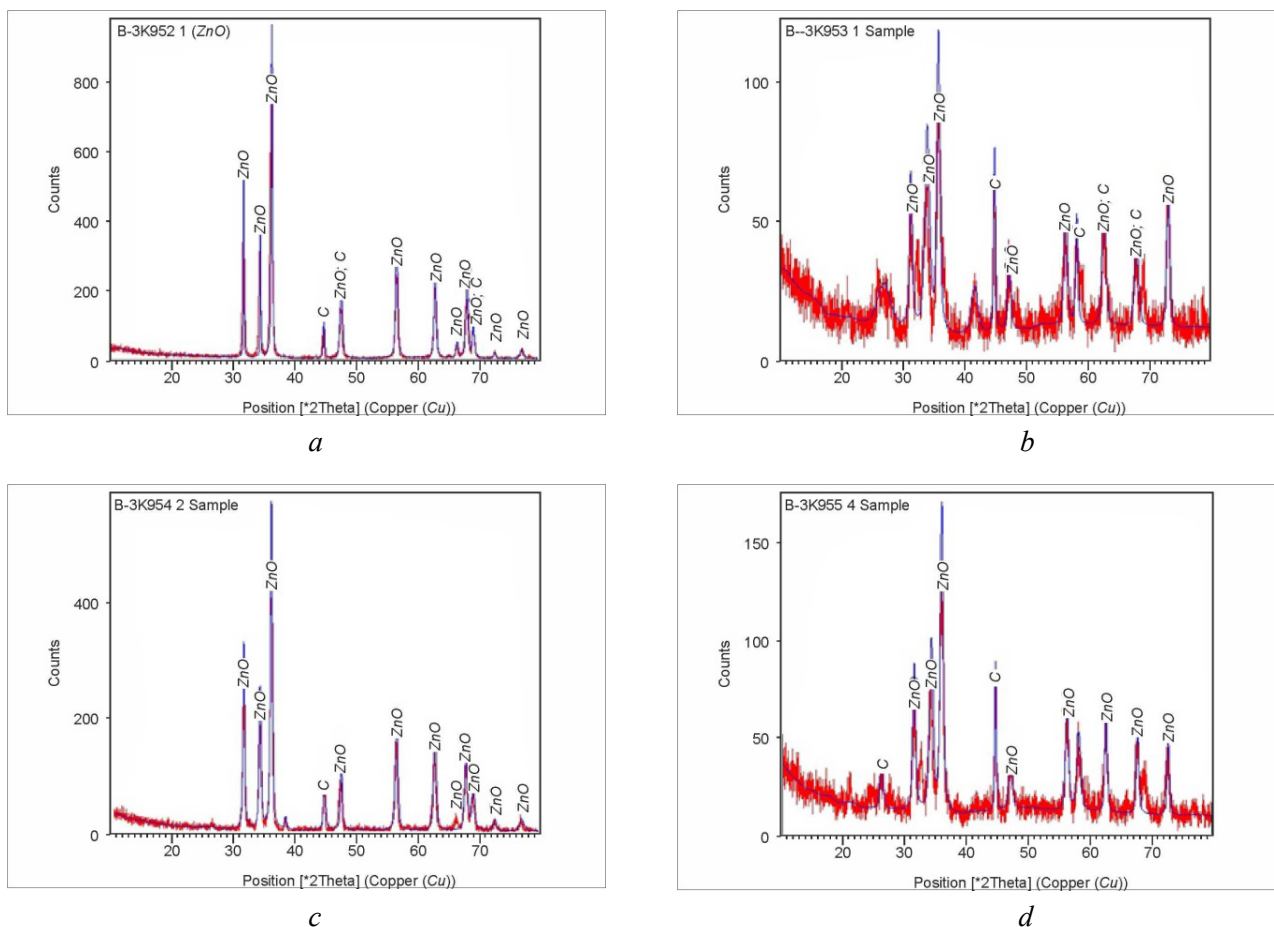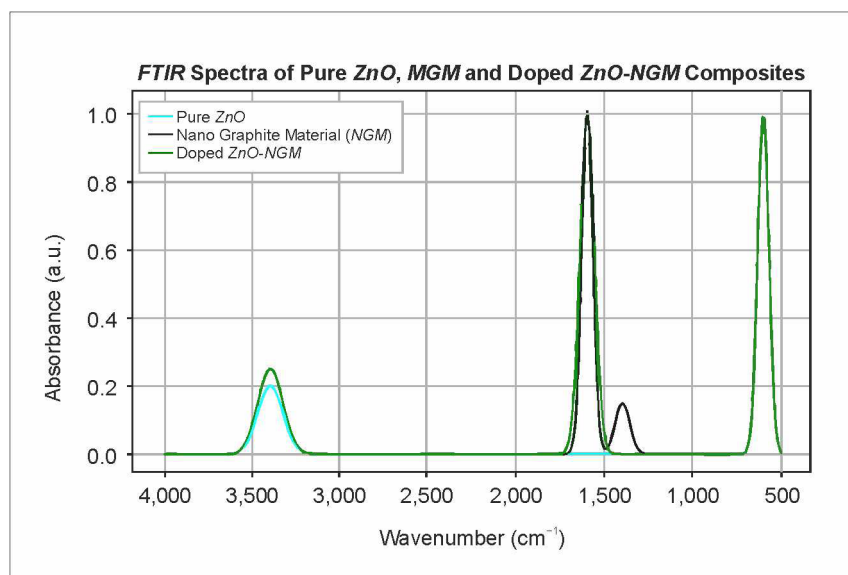*Fig. 4. XRD* patterns of (*a*) pure *ZnO*, (*b*) *ZnO–NGM* Sample 1, (*c*) Sample 2, and (*d*) Sample 3

*Fig. 5. FTIR spectra of pure ZnO, nanographite material (NGM),
and NGM-doped ZnO composites*

Doped *ZnO* showed characteristic *Zn–O* vibrations (400–600 cm^{-1}) and *O–H* stretching (~3,400 cm^{-1}). *NGM* spectra included *C=C* stretching (~1,600 cm^{-1}), *C–O* (~1,400 cm^{-1}), and *C–H* bending (~1,100–1,200 cm^{-1}), characteristic of sp²-hybridized carbon structures. Composites of *ZnO–NGM* showed shifted and intensified peaks, especially for *Zn–O* and *C=C*, indicating strong chemical bonding and successful doping. The broadened *O–H* peak indicated enhanced hydrogen bonding, which provided enhanced water affinity.

These microscopic and spectroscopic findings establish the successful integration of *NGM* into the *ZnO* structure. Increased surface area, lattice tension, and chemical functionalization enhance sensor performance and water adsorption. Decreased crystallite size and enhanced defect sites also enhance improved charge transport, which further increases the response rate and sensitivity of the humidity sensor.

The characteristic peaks of *ZnO*, *NGM*, and their composite indicate the presence of functional groups corresponding to *ZnO* vibrations and carbon-based materials. The shift in peak positions and intensity variations suggests successful doping of *NGM* into *ZnO*.

Electrical characterization and humidity sensing performance

To compare the electrical performance of the *ZnO–NGM* humidity sensors, a controlled humidity chamber was utilized. The sensor was positioned in a sealed chamber where humidity was accurately controlled from 10% to 90% *RH* using a dual-path nitrogen gas system. One path supplied nitrogen gas through a reservoir of distilled water to humidify it, while the other provided dry nitrogen to dehumidify it. The relative humidity was controlled by varying the flow rates of the two paths of nitrogen.

A digital hygrometer with ±0.8% *RH* accuracy was placed close to the sensor to continuously monitor *RH*, and the ambient temperature was held at 23 ± 1 °C. As shown in Fig. 6, the sensor was interfaced to a *Fluke PM6304/023* precision *LCR* meter with shielded terminals to reduce electrical noise. Automated data acquisition with real-time plotting and saving of capacitance values was carried out using a *Python*-based script. The capacitance of the sensor was recorded at 10 kHz, 20 kHz, 50 kHz, 80 kHz, 100 kHz, and 1 MHz frequencies under different humidity conditions.

The 2% *ZnO–NGM* sensor demonstrated a distinct monotonic increase in capacitance with RH. This was due to the adsorption of water molecules and increased dipolar polarization. The degree of doping made the sensor more sensitive than the pure *ZnO* because of the enhanced surface area and charge conduction pathways provided by the *NGM* flakes. The composite structure facilitated ionic conduction by adsorbed water layers and enhanced the dielectric constant via interfacial polarization. The response time was
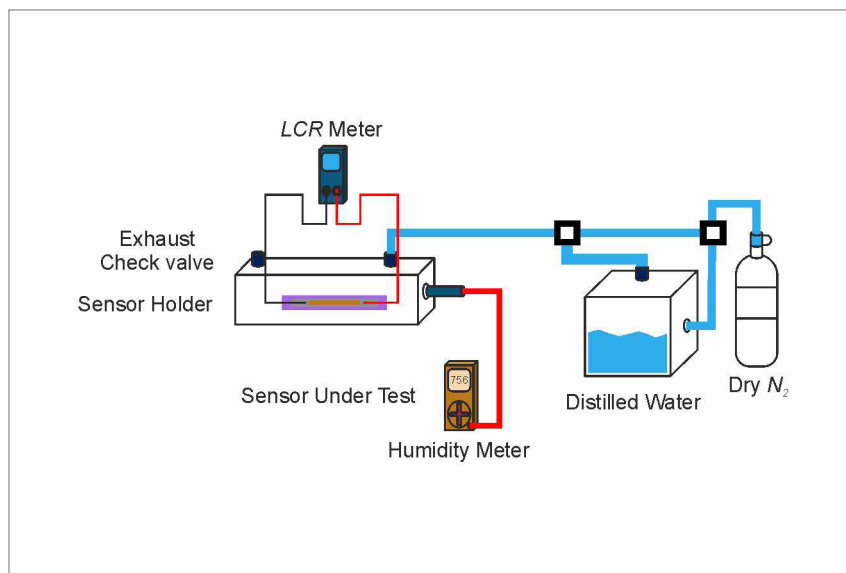
Fig. 6. Experimental setup for humidity sensing using an *LCR* meter
and a controlled chamber

4.5 seconds, and the recovery time was 6.9 seconds, reflecting efficient adsorption-desorption kinetics. As shown in Fig. 7, *a*, the capacitance-*RH* curve confirms moderate sensitivity and reliable humidity tracking at lower frequency ranges.

The 4% *ZnO–NGM* sensor exhibited well-balanced performance in sensitivity, response time, and recovery time. The capacitance rose steeply in the range of 10% to 60% *RH* and gradually at higher *RH*, with a good correlation between *RH* and capacitance. At lower frequencies (10–80 kHz), the sensor showed increased sensitivity as a result of improved dipole relaxation and ionic conduction, whereas at 1 MHz, the capacitance response became flattened as a result of polarization response time limitations. The response time was 4.0 s, and recovery time was 6.2 s, both of which were among the shortest recorded at all doping levels. As shown in Fig. 7, *b*, the capacitance-*RH* curve confirms moderate sensitivity and reliable humidity tracking at lower frequency ranges.

The 1% *ZnO–NGM* sensor had moderate capacitance sensitivity, response time, and recovery time. Capacitance increased with *RH* because of the dielectric polarization due to adsorbed water molecules. At lower frequencies (10 kHz and 50 kHz), the sensor was more sensitive, whereas at higher frequencies (1 MHz), the polarization response was restricted, leading to a flat capacitance curve. The response time was 4.8 seconds, and recovery time was 6.9 seconds, which provided a moderate improvement compared to the pure *ZnO*. As shown in Fig. 7, *c*, the capacitance-*RH* curve confirms moderate sensitivity and reliable humidity tracking at lower frequency ranges.

The 5% *ZnO–NGM* sensor exhibited high sensitivity to changing humidity levels, and the sensitivity was 53.9 pF/%*RH*. The capacitance rose sharply between 10% and 60% *RH* and gradually at higher *RH*. Although the sensor showed much higher sensitivity than with lower doping concentrations, the response and recovery times (4.2 and 6.6 seconds) were marginally slower as a result of partial agglomeration of the *NGM*, which lowered the number of active adsorption sites available. Despite the reduced kinetics, the sensor showed high sensitivity and was therefore appropriate for applications where sensitivity is more important than rapid response times. As shown in Fig. 7, *d*, the capacitance-*RH* curve confirms moderate sensitivity and reliable humidity tracking at lower frequency ranges.

The 10% *ZnO–NGM* sensor showed the highest capacitance sensitivity (62.1 pF/%*RH*) of all the doping levels, but its response time (6.0 s) and recovery time (8.0 s) were slower than those of the other sensors. The slower kinetics were mainly caused by the agglomeration of the *NGM* at this higher doping level, which restricted water molecule adsorption and desorption and also ionic mobility. Despite these limitations, the 10% doping level showed better sensitivity, and this is beneficial in many applications where sensitivity is important even at the cost of reduced response speed. As shown in Fig. 7, *e*, the capacitance-*RH* curve confirms moderate sensitivity and reliable humidity tracking at lower frequency ranges [31].
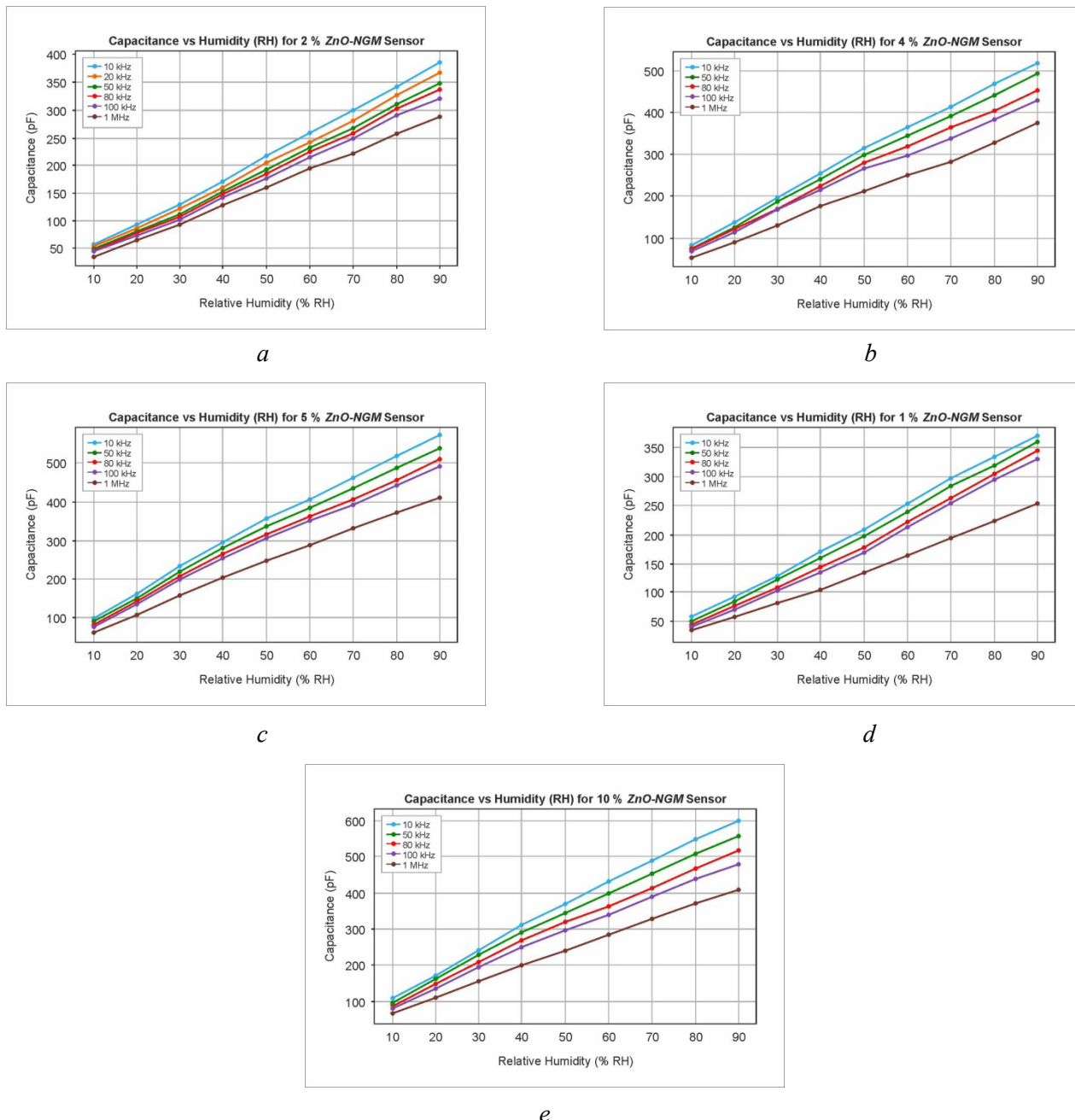
Fig. 7. Capacitance as a function of *RH* for *ZnO–NGM* sensors with (*a*) 2 wt.%, (*b*) 4 wt.%, (*c*) 1 wt.%, (*d*) 5 wt.%, and (*e*) 10 wt.% *NGM* doping

The dynamic behavior of the sensor was evaluated in terms of response and recovery time, which are defined as the time to achieve 90% of the maximum capacitance change when exposed to humidity and the time to recover to 10% of the initial value when moisture is removed, respectively (Table 1). The undoped *ZnO* had a response time of 5.0 s and a recovery time of 7.0 s. After doping, these values were significantly enhanced, and the 4% *ZnO–NGM* sensor realized an optimal trade-off: a quick response time of 4.0 s and a recovery time of 6.2 s. This is a characteristic of good water molecule adsorption–desorption kinetics facilitated by the synergy between *ZnO's* porous nature and *NGM's* charge transport ability.

At elevated *NGM* doping concentrations (≥5%), response and recovery times started to grow. For example, the 10% *ZnO–NGM* sensor had slower response (6.0 s) and recovery (8.0 s) times due to probable *NGM* agglomeration. Agglomeration decreases the number of active adsorption sites and inhibits water diffusion paths, thereby reducing sensing speed even though high capacitance sensitivity exists.

Capacitance variation with *RH* for different doping levels is shown in Fig. 8, *a*. While pure *ZnO* exhibited a baseline sensitivity of 18.5 pF/% *RH*, the introduction of *NGM* significantly enhanced the response.

**Effect of *NGM* doping on capacitance sensitivity, response time, and recovery time
of *ZnO*-based humidity sensors**

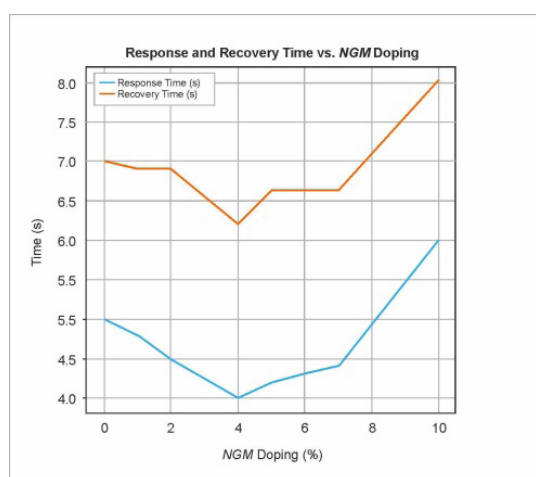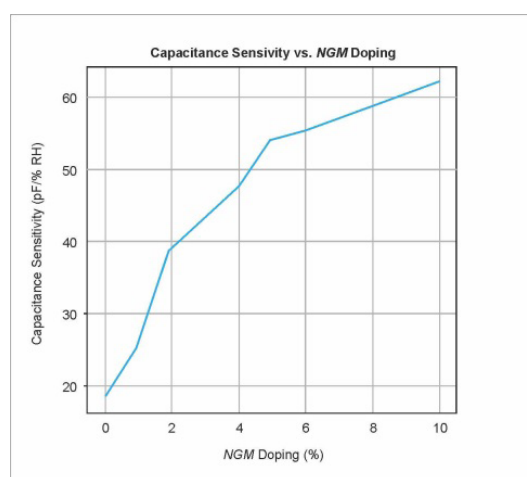| *NGM* Doping (%)	Capacitance sensitivity (pF/% RH)	Response time (s)	Recovery time (s)
0% (pure *ZnO*)	18.5	5	7
1 %	25.2	4.8	6.9
2 %	38.7	4.5	6.9
4 %	47.3	4.0	6.2
5 %	53.9	4.2	6.6
7 %	56.8	4.4	6.6
10 %	62.1	6	8

a

b

Fig. 8. (*a*) Response and recovery times as a function of *NGM* doping level; (*b*) Capacitance sensitivity
as a function of *NGM* doping level

Although 10% doping resulted in maximum sensitivity (62.1 pF/% *RH*), it came at the expense of slower kinetics. The 4% and 5% *ZnO-NGM* sensors presented the best compromise between high sensitivity and rapid response/recovery behavior, making them ideal candidates for real-time humidity detection.

ZnO-NGM-based humidity sensor response and recovery behavior was investigated to analyze real-time performance (Fig. 8, *b*). The best response (4.0 s) and recovery (6.2 s) times were obtained at 4% *ZnO–NGM*, due to the synergy between *ZnO's* high surface area and *NGM's* superior charge transport properties. For doping above 5%, performance decreased because *NGM* agglomeration decreased active adsorption sites and hampered electron mobility. At 10% doping, response and recovery times were elevated to 6.0 s and 8.0 s, respectively.

In general, controlled *NGM* doping greatly improves *ZnO* sensor performance, outperforming the drawbacks of conventional metal oxide sensors. The optimized *ZnO-NGM* composites surpass or match current sensors, showing great potential for use in environmental monitoring, industrial systems, and biomedical diagnostics. The cyclic sensing performance is indicated in Fig. 9, illustrating capacitance and *RH* levels against time over a period of 1,000 seconds. The capacitance (dotted red-blue line) closely follows the humidity (red squares), with evidence of synchronized and repeatable behavior.

The rapid slopes at times of humidity transition reflect rapid response and recovery behaviors. The regular periodic behavior supports sensor stability, repeatability, and suitability for dynamic environmental monitoring.
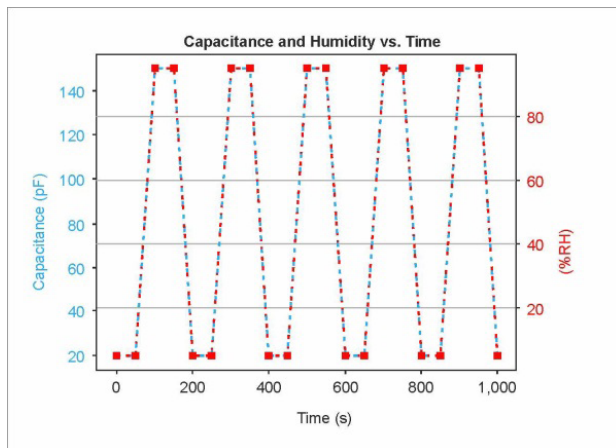
Fig. 9. Cyclic capacitance and humidity variation over 1,000 s, demonstrating sensor stability

Capacitive Sensitivity and Frequency Response

Capacitive sensitivity was greatly increased by *NGM* doping, reaching a peak of 65 a.u. for 5% NGM doping at 90% *RH* (Fig. 10, *c*). This is due to the high conductivity and high surface area of *NGM*, promoting increased charge storage and water molecule adsorption [8]. Doping concentrations higher than 5% caused decreased capacitance through agglomeration, limiting effective surface area and sites for adsorption.

Frequency-dependent measurements (Figs. 10, *a* and 10, *b*) identified that lower frequencies (<10 kHz) had more capacitance change, which is enhanced by stronger polarization. However, higher frequencies (>100 kHz) were less sensitive due to quicker charge carrier relaxation, restraining the capacity of water molecules to align with the electric field [9]. Fig. 7, *d* also verifies that at 5% doping, the sensor recorded high RH sensitivity over a range of frequencies, particularly at lower frequencies.
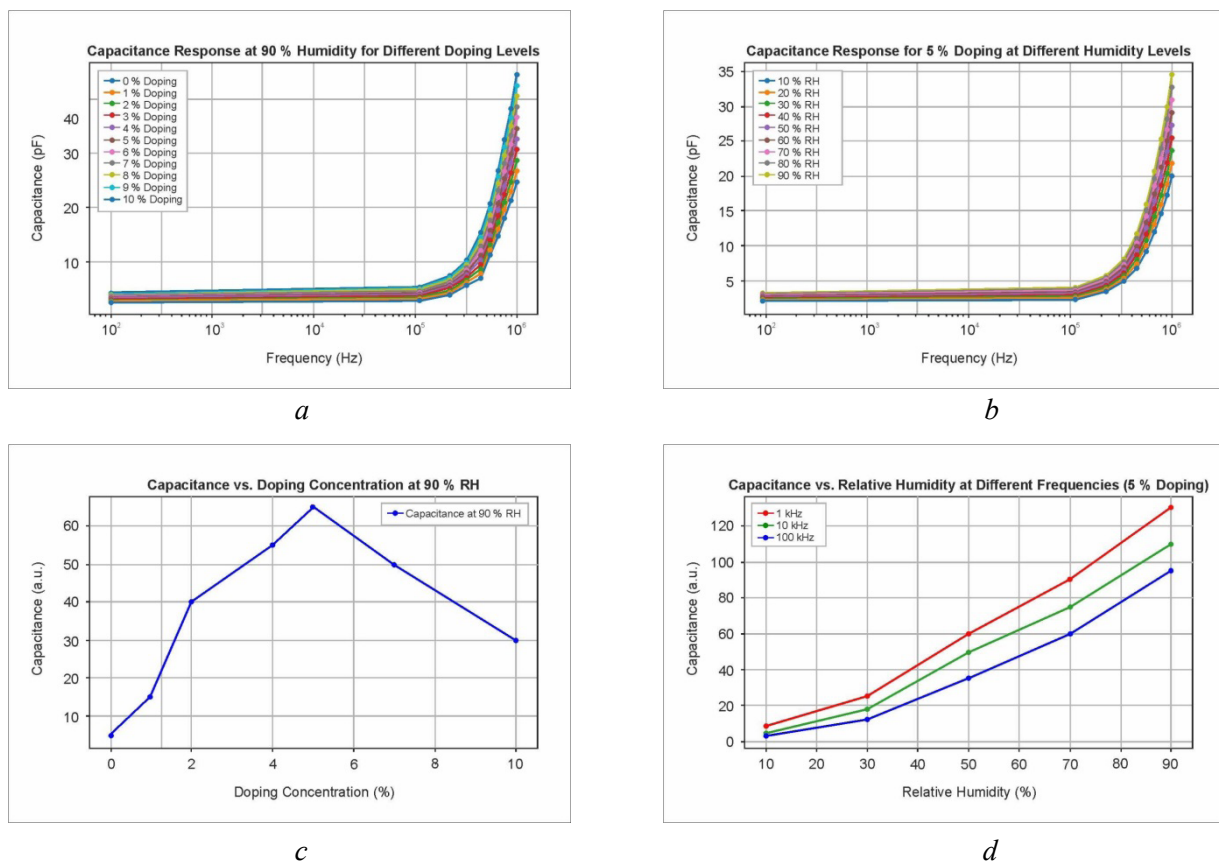

a

b

c

d

Fig. 10. (*a*) Capacitive response at 90% *RH*; (*b*) Response for 5 wt.% *NGM* doping; (*c*) Capacitance as a function of doping level at 90% *RH*; (*d*) Capacitance as a function of *RH* at different frequencies (5 wt.% *NGM* doping)

Electrode Influence on Sensor Performance

The influence of various electrode materials (*FTO*, silver, and copper) on sensor performance was assessed. *FTO* electrodes gave stable and reproducible responses, probably because of their chemical stability and strong adhesion to the sensing material. Silver electrodes improved sensitivity, probably because of their higher conductivity, which supports efficient charge transfer. Nevertheless, copper electrodes showed minor performance degradation with time, possibly because of oxidation effects, which can increase the contact resistance and lower the sensor sensitivity [32].

Comparison with existing sensors

Comparative studies between various humidity sensors emphasize the relative merits of *ZnO–NGM* sensors compared to multiple carbon-based and metal oxide-based materials. As an example, gram carbon quantum dot-based sensors have good sensitivity (178.6–254.86 pF/% *RH*) but less desirable response and recovery times (7.3–14.1 s) and therefore experience difficult detection at lower relative humidity (*RH*) concentrations. *PAA-MWCNT* composite sensors also register a notable resistance change (930 Ω) with humidity fluctuation but have very high response (680 s) and recovery (380 s) times, restricting their applicability. Graphene oxide (*GO*)-modified *PEDOT* sensors, though highly responsive to humidity (4.97% sensitivity at 97% RH), are characterized by sluggish response (31 s) and recovery (72 s). Other graphene-based sensors, including *Fe-GO* and *GO/WS$_2$* composites, offer modest performance but tend to have low sensitivity or high response/recovery times.

In order to put the performance of the *ZnO–NGM* humidity sensor prepared in the present research into perspective, its performance was compared to a vast array of recently published nanomaterial-based humidity sensors. Table 2 gives an overview of sensitivity, response time, recovery time, and some observations from past research work along with data from this research work.

The study shows that although some materials like gram carbon quantum dots have quite high sensitivity (178.6–254.86 pF/% *RH*), they have slow response and recovery times of up to 14.1 seconds, which restricts their use in fast-switching environments. Some designs, like the *PAA-MWCNT* composites, possess large resistance changes (930 Ω) but are weighed down by very long response (680 s) and recovery (380 s) times, making them unsuitable for real-time sensing.

Likewise, *GO*-modified *PEDOT* sensors exhibit a humidity sensitivity of 4.97% at 97% *RH* but with slower response (31 s) and recovery (72 s) cycles. *Fe–GO* and *GO/WS$_2$* sensors possess better speed but relatively lower sensitivity, particularly at lower *RH* values. Even *GO*-based sensors with abnormally high sensitivity (e.g., 37,800%) suffer from slow recovery times (~41 s) or are limited due to poor applicability in real-world situations because they are unstable at lower *RH*.

Conversely, *ZnO–NGM* sensors prepared in this work show a balanced and superior performance profile. The 5% *NGM*-doped *ZnO* sensor recorded a sensitivity of 53.9 pF/% *RH*, a response time of 4.2 s, and a recovery time of 6.6 s, outperforming many of the reported sensors with a significantly better dynamic response while retaining good sensitivity. At lower doping levels (e.g., 2% *NGM*), the sensor retained fast response (4.5 s) and recovery (6.9 s) times with a nominally lower sensitivity of 38.7 pF/% *RH*.

In addition, in contrast to most carbon-based sensors that exhibit scattered results across different *RH* levels, the *ZnO–NGM* sensors exhibited stable and reproducible performance within a broad *RH* range (10%–95%), rendering them feasible for application in real-time environmental or industrial monitoring systems. The fact that such sensors can also be made from inexpensive materials and using a facile doctor-blade method on *FTO* substrates further contributes to their practical benefits.

Structural and morphological analyses confirmed the successful incorporation of nanographite material (*NGM*) into the *ZnO* matrix. X-ray diffraction (*XRD*) patterns showed distinct peak shifts with increasing NGM content, indicating lattice strain and structural modification. Scanning electron microscopy (*SEM*) images revealed a uniform distribution of *NGM* within the *ZnO* matrix, resulting in increased surface roughness and the formation of additional active sites for water molecule adsorption. Fourier transform infrared (*FTIR*) spectroscopy further confirmed the presence of functional groups associated with humidity sensing, such as *O–H* stretching and *C=C* vibrations.

Ta b l e 2

Comparison of recent nano humidity sensors

No.	Sensor Material	Sensitivity (pF/%RH or %)	Response Time (s)	Recovery Time (s)	Reference	Key Observation
1	Gram Carbon Quantum Dots (*C-1*, *C-2*)	178.6–254.86	13.3 / 7.3	14.1 / 4.7	[33]	– High sensitivity; – Slow recovery
2	*PAA-MWCNT* (1:4 ratio)	930 Ом (resistance change)	680	380	[34]	– Excessively high response/recovery time
3	*GO*-modified *PEDOT*	4.97 % at 97 % RH	31	72	[35]	– Poor dynamic response
4	*MWCNT* in *NMP*	6.41	36	32	[36]	– Moderate performance
5	SnO_2–*RGO*	146.53	102	"several seconds"	[37]	– Slow at high *RH*
6	*GO*	37,800 %	10.5	41	[38]	– Very high sensitivity; – Long recovery
7	*Fe–GO*	5.18	31	11	[39]	– Low sensitivity at low *RH*
8	*GO*	–9.5 пФ/% *RH*	5	–	[40]	– Good speed; – Limited range
9	*GO*/WS_2 Composite	Not specified	11.3	12.4	[41]	– Stable performance 25–95% *RH*
10	CNT@CPM (Chitosan-PAMAM	Not specified	<20	<20	[42]	– Fast; – No sensitivity data
11	**5% ZnO–NGM (this work)**	**53.9**	**4.2**	**6.6**	this work	– Best balance; – High sensitivity; – Fast response
12	**2% ZnO–NGM (this work)**	**38.7**	**4.5**	**6.9**	this work	– Slightly lower sensitivity; – Still fast

Electrical characterization demonstrated that *NGM* doping significantly enhanced sensor performance. Among the samples, the *ZnO* sensor doped with 2% *NGM* exhibited the most favorable dynamic response, with a response time of 4.5 seconds and a recovery time of 6.9 seconds. This improvement is attributed to enhanced charge transport properties and a greater number of available adsorption sites. However, at higher doping concentrations (above 5%), although sensitivity increased, the response and recovery times became longer. This behavior is likely due to agglomeration effects, which reduce the effective surface area and hinder rapid adsorption-desorption kinetics.

A comparison with previously reported humidity sensors highlights the advantages of *ZnO-NGM* nanocomposites. While many conventional sensors suffer from slow response and poor recovery, the optimized doping concentration in this study achieved a desirable balance between sensitivity and speed. These enhancements suggest that *NGM*-doped *ZnO* sensors are promising candidates for real-time humidity monitoring across various domains, including industrial process control, environmental sensing, and biomedical diagnostics.

Future work should focus on further optimizing the doping concentration to enhance performance without compromising long-term stability. Additionally, exploring alternative film deposition techniques and integrating the sensor onto flexible substrates could enable the development of wearable or portable humidity sensors for next-generation smart systems.

Conclusions

This work reports the effective synthesis of *ZnO* nanoparticles doped with nanographite material (*NGM*) for high-performance capacitive humidity sensing. *UV–Vis* spectroscopy verified a strong absorption peak at 367 nm, confirming the semiconductor nature and optical suitability of the *ZnO* structure. Structural (*XRD*) and morphological (*SEM*) analyses showed enhanced crystallinity and surface texture, while *NGM* doping significantly improved adsorption kinetics and charge transport. Among the different doping levels that were tested, the 4% *NGM*-doped *ZnO* sensor had the best sensitivity-speed balance with a fast response time of 4.0 s and recovery time of 6.2 s. While doping levels of 5% and above provided higher capacitance sensitivity, the response speed was reduced, possibly due to agglomeration and lower active surface area. The sensors also exhibited very good repeatability, negligible hysteresis, and robust performance over a broad frequency and humidity range (10–95% *RH*, 10 kHz–1 MHz).

References

1. Saqib M., Ali Khan S., Mutee Ur Rehman H.M., Yang Y., Kim S., Rehman M.M., Young Kim W. High-performance humidity sensor based on the graphene flower/zinc oxide composite. *Nanomaterials*, 2021, vol. 11 (1), p. 242. DOI: 10.3390/nano11010242.

2. Yang H., Ye Q., Zeng R., Zhang J., Yue L., Xu M., Qiu Z.-J., Wu D. Stable and fast-response capacitive humidity sensors based on a ZnO nanopowder/PVP-RGO multilayer. *Sensors*, 2017, vol. 17 (10), p. 2415. DOI: 10.3390/s17102415.

3. Ullah Z., Mustafa G.M., Raza A., Khalil A., Awadh Bahajjaj A.A., Batool R., Sonil N.I., Ali I., Nazar M.F. Facile assembly of flexible humidity sensors based on nanostructured graphite/zinc oxide-coated cellulose fibrous frameworks for human healthcare. *RSC Advances*, 2024, vol. 14 (50), pp. 37570–37579. DOI: 10.1039/D4RA05761A.

4. Sun Y., Gao X., Shiwei A., Fang H., Lu M., Yao D., Lu C. Hydrophobic multifunctional flexible sensors with a rapid humidity response for long-term respiratory monitoring. *ACS Sustainable Chemistry & Engineering*, 2023, vol. 11 (6), pp. 2375–2386. DOI: 10.1021/acssuschemeng.2c06162.

5. Ding S., Yin T., Zhang S., Yang D., Zhou H., Guo S., Li Q., Wang Y., Yang Y., Peng B., Yang R., Jiang Z. Fast-speed, highly sensitive, flexible humidity sensors based on a printable composite of carbon nanotubes and hydrophilic polymers. *Langmuir*, 2023, vol. 39 (4), pp. 1474–1481. DOI: 10.1021/acs.langmuir.2c02827.

6. Wu K., Miao X., Zhao H., Liu S., Fei T., Zhang T. Selective encapsulation of ionic liquids in UiO-66-NH_2 nanopores for enhanced humidity sensing. *ACS Applied Nano Materials*, 2023, vol. 6 (10), pp. 9050–9058. DOI: 10.1021/acsanm.3c01727.

7. Lei D., Zhang Q., Liu N., Su T., Wang L., Ren Z., Zhang Z., Su J., Gao Y. Self-powered graphene oxide humidity sensor based on potentiometric humidity transduction mechanism. *Advanced Functional Materials*, 2022, vol. 32 (10), p. 2107330. DOI: 10.1002/adfm.202107330.

8. Adib M.R., Lee Y., Kondalkar V.V., Kim S., Lee K. A highly sensitive and stable rGO: MoS2-based chemiresistive humidity sensor directly insertable to transformer insulating oil analyzed by customized electronic sensor interface. *ACS Sensors*, 2021, vol. 6 (3), pp. 1012–1021. DOI: 10.1021/acssensors.0c02219.

9. Yu W., Chen D., Li J., Zhang Z. TiO_2-SnS_2 nanoheterostructures for high-performance humidity sensor. *Crystals*, 2023, vol. 13 (3), p. 482. DOI: 10.3390/cryst13030482.

10. Baig M.F.W., Hasany S.F., Shirazi M.F. Green synthesis of nano graphite materials from lemon and orange peel: A sustainable approach for carbon-based materials. *Engineering Proceedings*, 2023, vol. 46 (1), p. 42. DOI: 10.3390/engproc2023046042.

11. Dare E., Adanu-Ogbole B., Oladoyinbo F., Makinde F., Uzosike A.O. Synthesis and characterization of silver–zinc oxide nanocomposites for humidity sensing. *Nano Select*, 2023, vol. 4 (4), pp. 255–262. DOI: 10.1002/nano.202200106.

12. Mahjoub M.A., Monier G., Robert-Goumet C., Réveret F., Echabaane M., Chaudanson D., Petit M., Bideux L., Gruzza B. Synthesis and study of stable and size-controlled ZnO–SiO_2 quantum dots: Application as a humidity sensor. *The Journal of Physical Chemistry C*, 2016, vol. 120 (21), pp. 11652–11662. DOI: 10.1021/acs.jpcc.6b00135.

13. Qian L., Fang C., Gui Y., Tian K., Guo H., Guo D., Guo X., Liu P. Heterojunctions of ZnO-nanorod-decorated WO_3 nanosheets coated with ZIF-71 for humidity-independent NO_2 sensing. *ACS Applied Nano Materials*, 2023, vol. 6 (14), pp. 13216–13226. DOI: 10.1021/acsanm.3c01955.

14. Ling T.Y., Pu S.H., Fishlock S.J., Han Y., Reynolds J.D., McBride J.W., Chong H.M.H. Sensing performance of nanocrystalline graphite-based humidity sensors. *IEEE Sensors Journal*, 2019, vol. 19 (14), pp. 5421–5428. DOI: 10.1109/JSEN.2019.2905719.

15. Wu J., Yin C., Zhou J., Li H., Liu Y., Shen Y., Garner S., Fu Y., Duan H. Ultrathin glass-based flexible, transparent, and ultrasensitive surface acoustic wave humidity sensor with ZnO nanowires and graphene quantum dots. *ACS Applied Materials & Interfaces*, 2020, vol. 12 (35), pp. 39817–39825. DOI: 10.1021/acsami.0c09962.

16. Dinç Zor Ş., Cankurtaran H. Impedimetric humidity sensor based on nanohybrid composite of conducting poly (diphenylamine sulfonic acid). *Journal of Sensors*, 2016, vol. 2016 (1), p. 5479092. DOI: 10.1155/2016/5479092.

17. Lin C., Zhang H., Zhang J., Chen C. Enhancement of the humidity sensing performance in Mg-doped hexagonal ZnO microspheres at room temperature. *Sensors*, 2019, vol. 19 (3), p. 519. DOI: 10.3390/s19030519.

18. Chaudhary P., Verma A., Chaudhary S., Kumar M., Lin M.-F., Huang Y.-C., Chen K.-L., Yadav B.C. Design of a humidity sensor for a PPE kit using a flexible paper substrate. *Langmuir*, 2024, vol. 40 (18), pp. 9602–9612. DOI: 10.1021/acs.langmuir.4c00366.

19. Agadi N.P., Teradal N.L., Manjunatha D.H., Seetharamappa J. Zinc oxide anchored porous reduced graphene oxide: Electrode material for sensing of ezetimibe. *Journal of The Electrochemical Society*, 2024, vol. 171 (3), p. 037513. DOI: 10.1149/1945-7111/ad2f78.

20. Hongsith N., Chansuriya S., Yatmontree B., Uai S. Capacitively coupled contactless conductivity detection (C4D) of ZnO nanostructures gas sensor by adding Au: Pd metal with response to ethanol and acetone vapor. *Journal of Physics: Conference Series*, 2023, vol. 2653 (1), p. 012062. DOI: 10.1088/1742-6596/2653/1/012062.

21. Luo N., Cai H., Li X., Guo M., Wang C., Wang X., Hu P., Cheng Z., Xu J. Non-crystal-RuO$_x$/crystalline-ZnO composites: controllable synthesis and high-performance toxic gas sensors. *Journal of Materials Chemistry A*, 2022, vol. 10 (28), pp. 15136–15145. DOI: 10.1039/D2TA02856E.

22. Saxena K., Kumar A., Chauhan N., Khanuja M., Malhotra B.D., Jain U. Electrochemical immunosensor for detection of H. pylori secretory protein VacA on g-C$_3$N$_4$/ZnO nanocomposite-modified Au electrode. *ACS Omega*, 2022, vol. 7 (36), pp. 32292–32301. DOI: 10.1021/acsomega.2c03627.

23. Dhahri R., Benamara M., Nassar K.I., Elkenany E.B., Al-Syadi A.M. Zinc oxide-based sensor prepared by modified sol–gel route for detection of low concentrations of ethanol, methanol, acetone, and formaldehyde. *Semiconductor Science and Technology*, 2024, vol. 39 (11), p. 115021. DOI: 10.1088/1361-6641/ad825e.

24. Hussain S., Hasany S., Ali S.U. Hematite decorated MWCNT nanohybrids: A facile synthesis. *Journal of the Chemical Society of Pakistan*, 2022, vol. 44 (5), pp. 480–489. DOI: 10.52568/001121/JCSP/44.05.2022.

25. Doroftei C., Leontie L. Porous nanostructured gadolinium aluminate for high-sensitivity humidity sensors. *Materials*, 2021, vol. 14 (22), p. 7102. DOI: 10.3390/ma14227102.

26. Zhang H., Liu L., Huang C., Liang S., Jiang G. Enhanced acetone gas sensing performance of ZnO polyhedrons decorated with LaFeO$_3$ nanoparticles. *Materials Research Express*, 2023, vol. 10 (9), p. 095902. DOI: 10.1088/2053-1591/acf6f8.

27. Zhang D., Pan W., Zhou L., Yu S. Room-temperature benzene sensing with Au-doped ZnO nanorods/exfoliated WSe$_2$ nanosheets and density functional theory simulations. *ACS Applied Materials & Interfaces*, 2021, vol. 13 (28), pp. 33392–33403. DOI: 10.1021/acsami.1c03884.

28. Hosseini D., Donat F., Abdala P.M., Kim S.M., Kierzkowska A.M., Müller C.R. Reversible exsolution of dopant improves the performance of Ca$_2$Fe$_2$O$_5$ for chemical looping hydrogen production. *ACS Applied Materials & Interfaces*, 2019, vol. 11 (20), pp. 18276–18284. DOI: 10.1021/acsami.8b16732.

29. Fan W., Wang B., Gao R., Dimitrakopoulos G., Wang J., Xiao X., Ma L., Wu K., Yildiz B., Li J. Anodic shock-triggered exsolution of metal nanoparticles from perovskite oxide. *Journal of the American Chemical Society*, 2022, vol. 144 (17), pp. 7657–7666. DOI: 10.1021/jacs.1c12970.

30. Shah W., Khwaja R.W., Faraz S.M., Awan Z.H., Sayyad M.H. Photovoltaic and impedance analysis of dye-sensitized solar cells with counter electrodes of manganese dioxide and silver-doped manganese dioxide. *Engineering Proceedings*, 2023, vol. 46 (1), p. 31. DOI: 10.3390/engproc2023046031.

31. Zhang X., Maddipatla D., Bose A.K., Hajian S., Narakathu B.B., Williams J.D., Mitchell M.F., Atashbar M.Z. Printed carbon nanotubes-based flexible resistive humidity sensor. *IEEE Sensors Journal*, 2020, vol. 20 (21), pp. 12592–12601. DOI: 10.1109/JSEN.2020.3002951.

32. Al-Bonayan A.M., Althakafy J.T., Alorabi A.Q., Alamrani N.A., Aljuhani E.H., Alaysuy O., Al-Qahtani S.D., El-Metwaly N.M. Novel copper oxide-integrated carbon paste tirofiban voltammetric sensor. *ACS Omega*, 2023, vol. 8 (5), pp. 5042–5049. DOI: 10.1021/acsomega.2c07790.

33. Chaudhary P., Maurya D.K., Yadav S., Pandey A., Tripathi R.K., Yadav B.C. Ultrafast responsive humidity sensor based on roasted gram derived carbon quantum dots: experimental and theoretical study. *Sensors and Actuators B: Chemical*, 2021, vol. 329, p. 129116. DOI: 10.1016/j.snb.2020.129116.

34. Lee J., Cho D., Jeong Y. A resistive-type sensor based on flexible multi-walled carbon nanotubes and polyacrylic acid composite films. *Solid-State Electronics*, 2013, vol. 87, pp. 80–84. DOI: 10.1016/j.sse.2013.05.001.

35. Pang Y., Jian J., Tu T., Yang Z., Ling J., Li Y., Wang X., Qiao Y., Tian H., Yang Y., Ren T.-L. Wearable humidity sensor based on porous graphene network for respiration monitoring. *Biosensors and Bioelectronics*, 2018, vol. 116, pp. 123–129. DOI: 10.1016/j.bios.2018.05.038.

36. Kumar U., Yadav B.C. Development of humidity sensor using modified curved MWCNT based thin film with DFT calculations. *Sensors and Actuators B: Chemical*, 2019, vol. 288, pp. 399–407. DOI: 10.1016/j.snb.2019.03.016.

37. Zhang D., Chang H., Li P., Liu R., Xue Q. Fabrication and characterization of an ultrasensitive humidity sensor based on metal oxide/graphene hybrid nanocomposite. *Sensors and Actuators B: Chemical*, 2016, vol. 225, pp. 233–240. DOI: 10.1016/j.snb.2015.11.024.

38. Bi H., Yin K., Xie X., Ji J., Wan S., Sun L., Terrones M., Dresselhaus M.S. Ultrahigh humidity sensitivity of graphene oxide. *Scientific Reports*, 2013, vol. 3 (1), p. 2714. DOI: 10.1038/srep02714.

39. Kumar K., Kumar U., Singh M., Yadav B.C. Synthesis and characterizations of exohedral functionalized graphene oxide with iron nanoparticles for humidity detection. *Journal of Materials Science: Materials in Electronics*, 2019, vol. 30 (14), pp. 13013–13023. DOI: 10.1007/s10854-019-01663-9.

40. Zhao C.-L., Qin M., Li W.-H., Huang Q.-A. Enhanced performance of a CMOS interdigital capacitive humidity sensor by graphene oxide. *2011 16th International Solid-State Sensors, Actuators and Microsystems Conference*. IEEE, 2011, pp. 1954–1957. DOI: 10.1109/TRANSDUCERS.2011.5969243.

41. Wang G., Gao Q., Ke N., Si F., Wang J., Ding J., Zhang W., Fan X. Highly sensitive flexible humidity sensors with fast response and recovery times based on the composite of graphene oxide and WS 2 for detection of human breath and fingertip proximity. *Journal of Materials Chemistry C*, 2025, vol. 13 (10), pp. 4929–4937. DOI: 10.1039/D4TC05303F.

42. Kim H.-S., Kang J.-H., Hwang J.-Y., Shin U.S. Wearable CNTs-based humidity sensors with high sensitivity and flexibility for real-time multiple respiratory monitoring. *Nano Convergence*, 2022 , vol. 9 (1), p. 35. DOI: 10.1186/s40580-022-00326-6.

Conflicts of Interest

The authors declare no conflict of interest.